Title

Effective Removal of Anionic Re(VII) by Surface-Modified Ti2CT x MXene Nanocomposites: Implications for Tc(VII) Sequestration

Journal

Environmental Science and Technology, 53(7)

ISSN

0013-936X

Authors

Wang, Lin

Song, Huan

Yuan, Liyong

et al.

Publication Date

2019-04-02

DOI

10.1021/acs.est.8b07083

Peer reviewed

Effective Removal of Anionic Re(VII) by Surface-Modified Ti_2CT_x MXene Nanocomposites: Implications for Tc(VII) Sequestration

Lin Wang,[†,#] Huan Song,[†,‡,#] Liyong Yuan,[†] Zijie Li,[†] Peng Zhang,[†] John K. Gibson,[§] Lirong Zheng,[∥] Hongqing Wang,[‡] Zhifang Chai,[†,⊥] and Weiqun Shi*[,†]

[†]Laboratory of Nuclear Energy Chemistry and Key Laboratory for Biomedical Effects of Nanomaterials and Nanosafety, Institute of High Energy Physics, Chinese Academy of Sciences, Beijing 100049, China

[‡]School of Chemistry and Chemical Engineering and Hunan Key Laboratory for the Design and Application of Actinide Complexes, University of South China, Hengyang 421001, China

[§]Chemical Sciences Division, Lawrence Berkeley National Laboratory (LBNL), Berkeley, California 94720, United States

[∥]Beijing Synchrotron Radiation Facility, Institute of High Energy Physics, Chinese Academy of Sciences, Beijing 100049, China

[⊥]Engineering Laboratory of Advanced Energy Materials, Ningbo Institute of Industrial Technology, Chinese Academy of Sciences, Ningbo, Zhejiang 315201, China

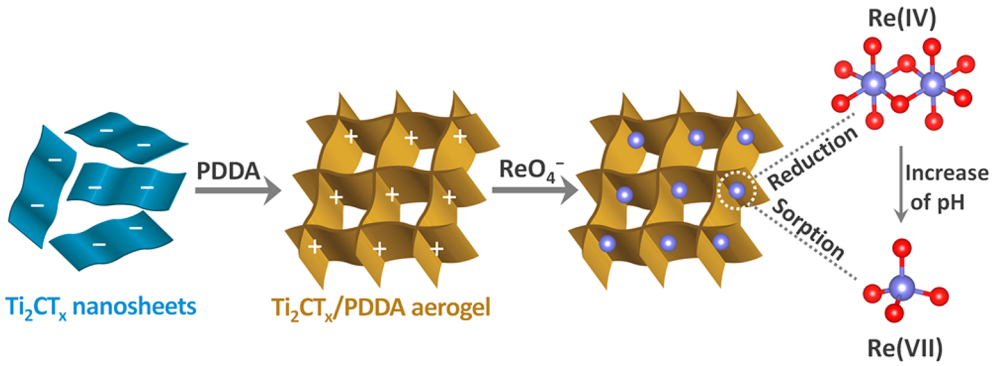

ABSTRACT: Environmental contamination by ^{99}Tc(VII) from radioactive wastewater streams is of particular concern due to the long half-life of ^{99}Tc and high mobility of pertechnetate. Herein, we report a novel MXene-polyelectrolyte nanocomposite with three-dimensional networks for enhanced removal of perrhenate, which is pertechnetate simulant. The introduction of poly(diallyldimethylammonium chloride) (PDDA) regulates the surface charge and improves the stability of Ti_2CT_x nanosheet, resulting in Re(VII) removal capacity of up to 363 mg g^{-1}, and fast sorption kinetics. The Ti_2CT_x/PDDA nanocomposite furthermore exhibits good selectivity for ReO_4^- when competing anions (such as Cl^- and SO_4^{2-}) coexist at a concentration of 1800 times. The immobilization mechanism was confirmed as a sorption-reduction process by batch sorption experiments and X-ray photoelectron spectroscopy. The pH-dependent reducing activity of Ti_2CT_x/PDDA nanocomposite toward Re(VII) was clarified by X-ray absorption spectroscopy. As the pH increases, the local environment gradually changes from octahedral-coordinated Re(IV) to tetrahedral-coordinated Re(VII). The overall results suggest that Ti_2CT_x/PDDA nanocomposite may be a promising candidate for efficient elimination of Tc contamination. The reported surface modification strategy might result in applications of MXene-based materials in environmental remediation of other oxidized anion pollutants.

INTRODUCTION

Technetium-99 (^{99}Tc), a β decay emitter produced from nuclear fission of ^{235}U and fabrication of weapon grade plutonium, is a particularly problematic radionuclide in legacy nuclear waste due to long half-life (2.13×10^5 years) and high thermal neutron fission yield (6.1%).[1,2] In oxygenated aqueous solutions, Tc is usually present as Tc(VII) in the form of pertechnetate anion, TcO_4^-.[3,4] Because of high water solubility and low retention on soil and natural minerals, TcO_4^- exhibits a high environmental mobility, which results in Tc-contamination around nuclear waste reprocessing and storage sites.[5−7] Accordingly, there is need for efficient and rapid removal of Tc(VII) from radioactive environmental wastewater, which is a challenging task.

Several types of solid sorbents have been explored for the remediation of Tc(VII) and other toxic anions, including layered double hydroxides (LDHs),[8,9] activated carbon,[10] ion-exchange resins,[11,12] functionalized polymers,[13−15] porous aromatic

frameworks,[16] and metal organic frameworks (MOFs).[17−20] For instance, Wang et al. synthesized a water-stable and radiation-resistant cationic MOF, SCU-101, that selectively recognizes TcO_4^- via strong hydrogen-bond interactions.[21] As an alternative to ion-exchange, a promising strategy for Tc remediation is reduction of Tc(VII) to insoluble and relatively immobile Tc(IV).[22] Techniques including radiolysis reduction (via γ radiation in alkaline solution),[23,24] bioreduction,[5,25,26] photoreduction,[27] and electroreduction[28,29] have been developed for Tc(VII) immobilization. Chemical reduction is attractive due to ease of implementation, rapid kinetics, and low cost. Current candidate solid reduction agents focus on a handful of materials including zerovalent iron,[30,31] Fe(II)-containing compounds,[22,32] sulfides,[33,34] Sn(II/IV) phosphate,[35] and composites of these constituents. Limitations of Tc(VII) reductants include low removal capacity and poor selectivity, and novel materials with reductive activity and sequestration capacity for Tc(VII) remain a goal.

Two-dimensional transition metal carbide (MXene) is a new class of layered nanomaterials that has emerged in the energy and environmental fields due to intriguing physicochemical properties.[36−39] In particular, it has been demonstrated that multilayered MXenes are promising candidates for cleanup of several radionuclide cations (e.g., $^{238}UO_2^{2+}$, $^{232}Th^{4+}$, $^{133}Ba^{2+}$, and $^{107}Pd^{2+}$) by versatile interaction pathways that include coordination, ion exchange, and reduction immobilization.[40−45] For sequestration of anions such as $UO_2(CO_3)_3^{4-}$ and ReO_4^-, MXenes are generally ineffective due to their intrinsically negatively charged surfaces and the limited number of active sites on multilayer structures.[40] Although effective anion adsorption and reduction by MXenes has been demonstrated under very acidic conditions, when the surface charge becomes positive,[46,47] the narrow useful pH range may restrict practical environmental applications. A straightforward strategy to overcome this challenge is regulation of MXene surface properties through hybridization and modification. Herein, we report a simple, cost-effective and scalable method to fabricate Ti_2CT_x/poly(diallyldimethylammonium chloride) (PDDA) nanocomposites for enhanced removal of ReO_4^- from aqueous solutions. There components were chosen because Ti_2CT_x is a highly active MXene with reducing capability, and PDDA is a common cationic polyelectrolyte that is widely used in water treatment and mining.[48,49] ReO_4^- is sufficiently chemically similar to TcO_4^- to serve as a nonradioactive surrogate, though extrapolation from ReO_4^- to TcO_4^- must be judicious.[50−52] In the present work, different morphologies of Ti_2CT_x (multilayered or nanosheet MXene) and their nanocomposites with PDDA were synthesized and characterized. Re(VII) removal was evaluated by batch sorption and anion competition experiments. The removal mechanisms were clarified using X-ray absorption spectroscopy and photoelectron spectroscopy.

EXPERIMENTAL DETAILS

Synthesis of Ti_2CT_x and Its Composites. 4.07 g LiF was added to 66.7 mL of 7.5 M HCl and stirred for several minutes to yield a transparent solution. 2.4 g Ti_2AlC powder was added in batches of ca. 80 mg each during 20 min, after which the solution was stirred at 35 °C for 72 h to ensure complete etching of Al. The product was washed with deionized water and centrifuged for 5 min at 3500 rpm. The wash/centrifuge cycle was repeated until a stable dark-red supernatant was obtained, indicating a spontaneous delamination of Ti_2CT_x MXene. Finally, deionized water was added, followed by shaking and centrifugation at 2000 rpm for 30 min to collect the colloidal solution of Ti_2CT_x nanosheets (TCNS). The concentration of LiF (C_{LiF}, optimized here as 2.35 M) is a key parameter for high-yield synthesis of TCNS (~80 wt % yield based on added Ti_2AlC). No delamination was evident for C_{LiF} less than 2.3 M, presumably indicating this as the minimum concentration of Li^+ needed to sufficiently weaken the interaction between MXene interlayers.[53] Higher C_{LiF} (e.g., 2.7 M) resulted in continued dissolution of TCNS and formation of Li_3AlF_6 impurity. The synthesis of multilayerd Ti_2CT_x (MTC) was as reported previously,[40] using C_{LiF} = 1M.

The Ti_2CT_x nanosheet/PDDA composite (TCNS-P) was synthesized by dropwise addition of 100 mL 2 wt % PDDA (M_w = 100 000−200 000) aqueous solution into 100 mL TCNS colloidal solution (10 mg mL^{-1}) under vigorous stirring. The mixture was further stirred for 2 h under argon, after which the sediment was centrifuged at 10 000 rpm and washed with deionized water for three cycles to remove excess PDDA. A black aerogel cake of TCNS-P was obtained by drying the gel-like product in a freeze-dryer at −60 °C for 48 h (Supporting Information (SI) Figure S1). The composite of multilayered Ti_2CT_x/PDDA (MTC-P) was prepared by this same procedure, but using MTC instead of TCNS.

Batch Sorption Experiments. Re(VII) sorption experiments were conducted in an anaerobic glovebox at 303 K. In a typical procedure, 8 mg sorbent sample was added to 20 mL of 100 mg L^{-1} Re(VII) (NH_4ReO_4, Sinopharm Chemical Reagent Co. Ltd.). After adding 0.1 M NaOH or 2 M HCl to adjust the pH, the suspension was shaken slightly for about 48 h to ensure equilibrium adsorption and reduction of Re(VII). The supernatant was then separated by centrifugation at 10 000 rpm, and diluted with 5 wt % HNO_3 to ensure that the concentration of Re(VII) was in the range of 1−5 mg L^{-1}. The residual solution concentration of Re(VII) was measured using inductively coupled plasma-optical emission spectrometry (ICP-OES, Horiba JY 2000−2, detection limit below 0.01 mg L^{-1}). The removed Re(VII) (q_e) was calculated by the following equation: $q_e = (C_0 - C_e)V/m$, where C_0 and C_e are the initial and equilibrium concentrations of Re(VII), m is the sorbent mass, and V is the solution volume. Concentrations of 10 and 100 mmol L^{-1} Na_2SO_4, NaCl, $NaClO_4$, or $NaNO_3$ were employed to evaluate effects of competitive anions on Re(VII) removal.

X-ray Absorption Spectroscopy. XANES and EXAFS spectra at the Re L_3 absorption edge (~10 535 eV) were collected at beamline 1W1B of the Beijing Synchrotron Radiation Facility (BSRF). The ReO_2 reference spectrum was measured in transmission mode, and spectra of the aqueous Re(VII) reference and other samples were measured in fluorescence mode. XANES and EXAFS data were pre-edge background subtracted, normalized, and fitted by the Athena and Artemis programs in the IFEFFIT package.[54] A k range of ~3.0−13.0 $Å^{-1}$ and Rbkg 1.1 were used to obtain the Fourier transform of Re L_3 k^3-weighted spectra. Four scattering pathways (Re−O_1, Re−Re, Re−O_{MS}, and Re−O_2, nomenclature explained below) based on the crystal structures of ReO_2 and $KReO_4$ were used to calculate the theoretical phase and amplitudes for the extraction of metric parameters from EXAFS data. All fitting operations were performed in R space of ~1.1−4.0 Å. The amplitude reduction factor (S_0^2) was set to 0.83 as determined from EXAFS analysis of reference samples.

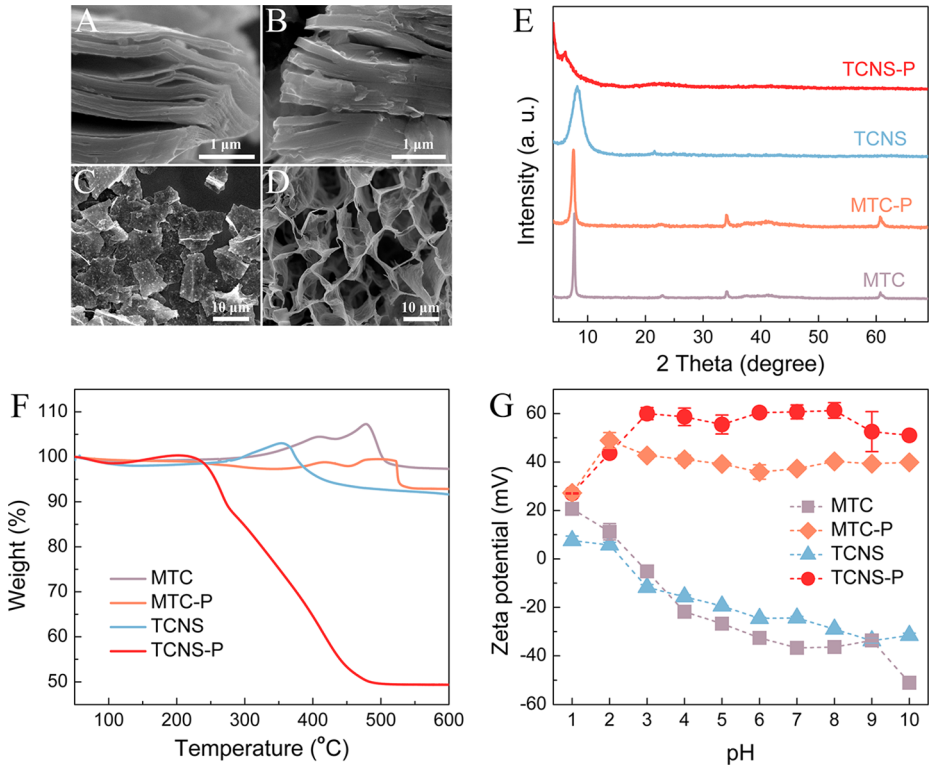

Figure 1. SEM images (A–D), powder XRD patterns (E), thermogravimetric weight-loss curves (F), and zeta potentials versus solution pH (G) of Ti_2CT_x and its nanocomposites. (A) MTC; (B) MTC-P; (C) TCNS; (D) TCNS-P.

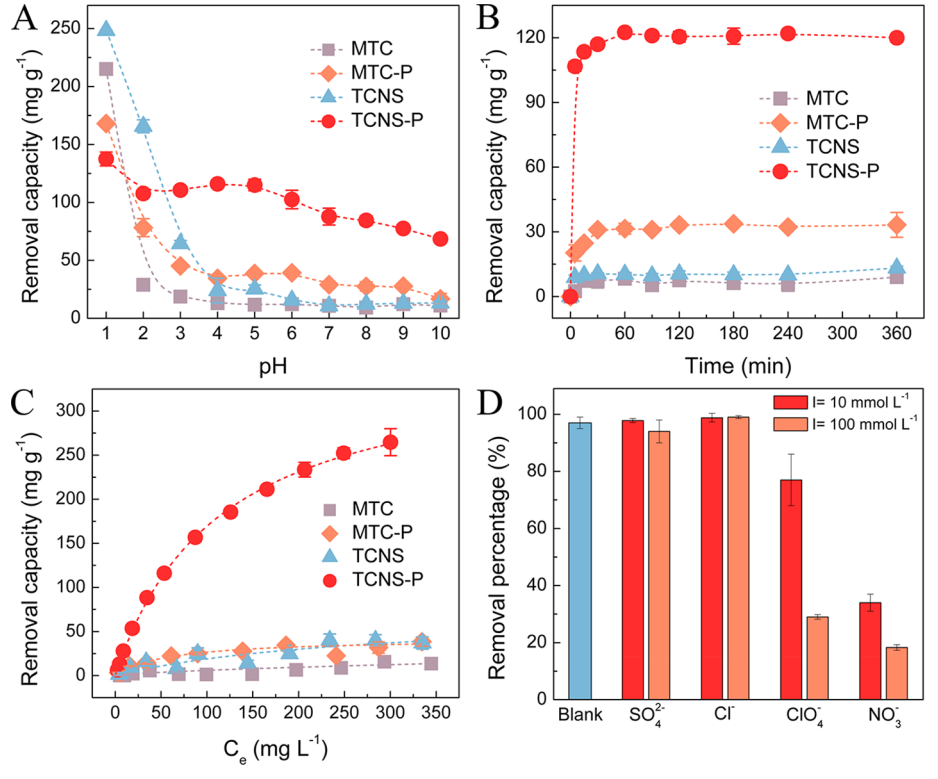

Figure 2. (A–C) Re(VII) removal from aqueous solution by Ti_2CT_x and PDDA hybrids as a function of pH, contact time and equilibrium Re(VII) concentration. (D) Effect of competitive anion species on Re(VII) removal by TCNS-P. Experimental parameters: (A) m/V = 0.4 g L^{-1}, C_0 = 100 mg L^{-1}; (B) pH 4.0 ± 0.1, m/V = 0.4 g L^{-1}, C_0 = 100 mg L^{-1}; (C) pH 4.0 ± 0.1, m/V = 0.4 g L^{-1}, C_0 = 5–400 mg L^{-1}; (D) pH 4.0 ± 0.1, m/V = 0.75 g L^{-1}, C_0 = 10 mg L^{-1}, I = 10 or 100 mmol L^{-1}.

RESULTS AND DISCUSSION

Characterization of Ti_2CT_x and Its Composites. The morphologies of as-synthesized Ti_2CT_x and its composites are shown in Figure 1A–D. MTC and MTC-P have a typical graphite-like stacking structure. TCNS is dispersed nanosheets from delamination of multilayered Ti_2CT_x under high concentration of Li^+. After interaction with PDDA, the nanosheets are assembled into a porous three-dimensional network with a pore size around 10 μm (Figure 1D). The Brunauer–Emmett–Teller (BET) surface area of TCNS-P is 18 $m^2 g^{-1}$ (SI Figure S2), which is larger than that for MTC-P (5 $m^2 g^{-1}$), but smaller than that for TCNS (31 $m^2 g^{-1}$) probably due to coating and linking of nanosheets by PDDA. Powder XRD results for the four samples are shown in Figure 1E. The (002) peak at ~7.8° for MTC, which is consistent with the literature,[40] is slightly shifted to 7.6° for MTC-P. For TCNS, the broadening of the (002) peak and disappearance of the nonbasal (110) peak at 61° indicate successful exfoliation of Ti_2CT_x lamellas. Formation of TCNS-P from TCNS and PDDA results in a significant decrease in diffraction intensity and a (002) peak shift from 8.2° to 6.1°, which corresponds to an increase of *d*-spacing from 10.8 to14.5 Å. These results reveal a highly disordered nature of TCNS-P and the intercalation of some PDDA molecules inside few-layered Ti_2CT_x nanosheets. The FTIR spectra in SI Figure S3 also demonstrate co-incorporation of PDDA and Ti_2CT_x in TCNS-P, as indicated by PDDA C=C modes at 1474 cm^{-1} and C–H stretches at 2952 cm^{-1},[48,55,56] and the Ti–O MXene band at 560 cm^{-1}.[57] TGA measurements provide estimated PDDA contents of 4% and 45% in MTC-P and TCNS-P, respectively (Figure 1F). The weight gain of MTC, MTC-P, and TCNS in temperature range of 350–500 °C corresponds to the oxidation of Ti_2CTx MXene under air atmosphere. TCNS exhibits a lower oxidation temperature than MTC and MTC-P, suggesting the higher reactivity of nanosheet MXene. Surface modification of Ti_2CT_x MXene with PDDA was further confirmed by zeta potential data, as shown in Figure 1G. Pristine MXenes MTC and TCNS have similar zero charge points (around pH 2–3), with their zeta potentials becoming more negative as pH increases, presumably due to $Ti–O^-$ groups on MXene surface for pH > 3.0. In contrast, MTC-P and TCNS-P exhibit positively charged surfaces over the entire studied pH range of 1.0–10.0. The larger positive zeta potential of TCNS-P versus MTC-P (e.g., + 59 mV vs +41 mV at pH 4.0), suggests that the morphology of superthin nanosheets facilitates functionalization of Ti_2CT_x by PDDA.

Batch Sorption Experiments. Figure 2A shows removal of Re(VII) by the four MXene samples as a function of pH. All samples exhibit a high Re(VII) removal capacity at acidic pH 1.0, presumably because a positively charged Ti_2CT_x surface facilitates electrostatic interaction with Re(VII) anions. As discussed below, the high reactivity of Ti_2CT_x allows reduction of Re(VII), accompanied by consumption of protons from aqueous solutions,[29] with the result that high acidity can promote reduction and thus removal of Re(VII) as Re(IV). However, such acidic pH has the adverse effect of Ti_2CT_x MXene dissolution (ca. 55–60% at pH 1.0 based on Ti content, SI Figure S4). SI Figure S4 also indicates that the PDDA component in TCNS-P greatly suppresses dissolution at pH > 2.0, thereby improving Ti_2CT_x nanosheet stability. The drastic decrease in removal capacity for MTC and TCNS with increasing pH above 1.0 (Figure 2A) is attributed to electrostatic repulsion between negative surface of MXene and anionic Re(VII). Modification by PDDA enables MXene to exhibit a positively charged surface nearly independent of pH, which results in attraction between TCNS-P and Re(VII) over the entire pH range of 1–10 (Figure 2A). In contrast to pH-independent high Re(VII) uptake by TCNS-P, the uptake by MTC-P decreases rapidly with increasing pH despite an apparently positive surface. The very similar XRD patterns of MTC-P and MTC (Figure 1E) suggest that modification by PDDA occurs only on the exposed exterior surface of MTC, probably due to the small interlayer spacing that renders the multilayered structures inaccessible to PDDA. The unmodified surfaces inside MTC-P may thus remain negatively charged at high pH, which hinders diffusion and uptake of Re(VII) anions.

Kinetic experiments were conducted to evaluate the removal rate and controlling mechanism for Re(VII) uptake. As illustrated in Figure 2B, Ti_2CT_x and its composites exhibit rapid sorption kinetics, with equilibration in less than 1 h. Kinetic fitting parameters based on pseudo-first-order and pseudo-second-order models are in SI Table S2, where it is apparent that the latter model distinctively provides high correlation coefficients and also removal capacities in good accord with the experiment. The kinetic results indicate that removal of Re(VII) by Ti_2CT_x and its composites is controlled primarily by chemisorption, rather than by mass transport.[58,59] Particularly noteworthy is that the Re(VII) removal capacity of TCNS-P is an order of magnitude higher than that of TCNS or MTC (Figure 2B), as a result of surface modification and more efficient utilization of interaction sites.

Figure 2C shows sorption isotherms of Re(VII) for the MXene materials. The isotherms were fitted using the Langmuir and Freundlich models with fitting parameters as summarized in SI Table S3. The correlation coefficients reveal that Re(VII) sorption on the PDDA modified MXenes, TCNS-P, and MTC-P, is well fit by Langmuir model, while sorption by pristine MXenes, TCNS, and MTC, is better represented by Freundlich model. Heterogeneous adsorption of Re(VII) on TCNS and MTC is attributed to various active MXene surface sites, such as terminating groups –OH, –O, –F, and – Cl.[40,41,60] Introduction of PDDA screens these functional groups, with the result that electrostatic attraction of Re(VII) by quaternary ammonium cations on the polyelectrolyte PDDA backbone becomes dominant, which is better represented by Langmuir model. It is evident from the results in Figure 2 that, for the studied concentration range, TCNS-P exhibits a great enhancement in removal capacity compared to the other MXene samples. The maximum sorption capacity of TCNS-P, estimated as 363 mg g^{-1}, is higher than, or at least comparable to, traditional nanosorbents and ion-exchange resins (SI Table S4).

To assess the potential efficacy of TCNS-P in environmental applications, we investigated effects of different types and concentrations of competitive anions on Re(VII) removal at pH 4.0. The results in Figure 2D demonstrate that TCNS-P can remove at least 94% of Re(VII) even in the presence of a 1860 times higher concentration of SO_4^{2-} or Cl^-. The resulting distribution coefficient, K_d, is >2.1×10^4 mL g^{-1}, which indicates that TCNS-P is a promising candidate to efficiently remove Re(VII) from wastewater containing excess of competing anions. It is apparent in Figure 2D that competing ClO_4^- substantially suppresses uptake of Re(VII), probably due to the similar structures, ionic radii and hydration energies of ClO_4^- and ReO_4^-.[8,61,62] Nevertheless, the removal percentage of Re(VII) still remains at 77% in the presence of excess ClO_4^- at a moderate ionic strength of 10 mmol L^{-1}. Zhang et al. found

that the affinity of quaternary amine for anions followed the same order with our our results, namely, perchlorate ≫ sulfate > chloride.[63] Roach et al. also reported high perchlorate retentions of PDDA in simulated groundwater containing chloride and sulfate.[64] We conjecture that the alkyl backbone of PDDA may provide a weak hydrophobic environment to stabilize perrhenate/perchlorate with low hydration energies. On the other hand, Re(VII) could be simultaneously reduced by Ti_2CT_x MXene under pH 4.0 (see below), thus promoting the selectivity of TCNS-P to perrhenate. Apparent in Figure 2D is that the presence of competing NO_3^- more drastically inhibits Re(VII) removal, which may be related to the oxidizing properties of nitrate (redox potential = +0.96 V).[65] Maset et al. reported the recalcitrance of Re(VII) under nitrate-containing biogeochemical reduction conditions, which is consistent with our results.[7] Upon increasing the amount of adsorbent from 0.75 g L^{-1} to 5 g L^{-1} under nitrate conditions, Re(VII) removal increased from about 30% to nearly 60% (SI Figure S5). The effect of competing anions on Re(VII) uptake at pH 2.0 (SI Figure S6) follows the same trend as at pH 4.0: NO_3^- (most inhibiting) > ClO_4^- > SO_4^{2-} ≈ Cl^- (least inhibiting).

Speciation of Rhenium and Removal Mechanism. To evaluate oxidation state information of rhenium in TCNS-P samples at different pH, the Re L_3 edge XANES spectra shown in Figure 3 were acquired. The 1.8 eV energy shift for the strongest XANES absorption resonance (i.e., the "white line") between Re(IV) and Re(VII) is in good agreement with literature results.[66] In the acidic pH range of 1.0−4.0, the white line energies for rhenium-containing samples are close to that of ReO_2, indicating predominantly reduction of Re(VII) to Re(IV) by TCNS-P. At pH 4.0, the white line energy is ~0.4 eV higher than for ReO_2, revealing partial reduction of Re(VII). At neutral pH 7.0, the white line position indicates only minor reduction of Re(VII), and a pH 10.0 there is negligible reduction. In addition to the white line, the changes in less intense XANES features in the range 10 570−10 650 eV also indicate Re oxidation state. In particular, the weak absorption resonance at 10588 eV suggests an oxidation state closer to Re(IV) under acidic conditions. Under neutral and alkaline conditions, the 10 588 eV resonance is replaced by a broadened peak around 10 613 eV, consistent with Re(VII) reference. Oxidation state fractions were estimated from a comparison of the measured absorption edge energy (E_0) with a linear interpolation between ReO_2 and ReO_4^- (SI Table S1). The estimated fraction of Re(IV) decreases from 89% to 22% as the solution pH increases from 3.0 to 7.0. The overall XANES results indicate that reduction of aqueous Re(VII) to Re(IV) by TCNS-P is strongly pH dependent.

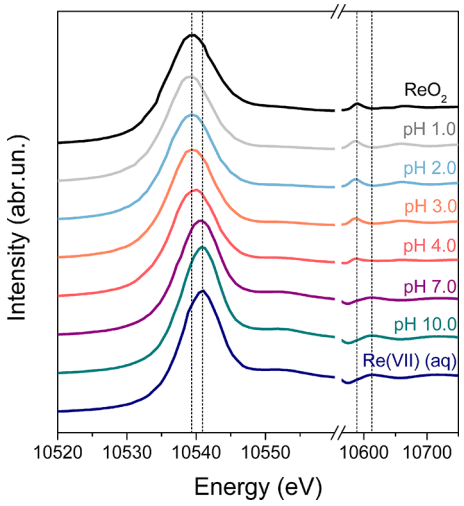

Figure 3. Re L_3 edge XANES spectra of rhenium-containing TCNS-P samples for different solution pH. Re L_3 edge XANES spectra of Re(IV) and Re(VII) references are shown for comparison.

EXAFS data can elucidate the local structure around metal atoms.[67,68] Figure 4 shows Re L_3 edge k^3-weighted spectra, along with their Fourier transforms (FT) and the corresponding fitting results. The differing oscillation periods for low-k (k < 7 $Å^{-1}$) in Figure 4A under acidic and basic conditions suggest different first coordination shells around Re. FT fitting (Figure 4B and Table 1) shows that under acidic conditions there are six O atoms at 2.03 Å (Re−O_1) and a Re−Re distance of 2.58 Å, which are consistent with distances of Re−O (2.01 Å) and Re−Re (2.57 Å) in octahedral-coordinated ReO_2. The absence of multiple scattering interactions (Re−O_{MS}) in samples for pH 1.0−4.0 may be due to asymmetrical octahedral structures. The coordination number (N) of Re−Re is close to 2.0, indicating the formation of ReO_2 one-dimensional chains in an edge-sharing fashion.[1,23] A significantly shorter Re−O bond with a distance of 1.74 Å (Re−O_2) is observed for alkaline conditions (pH 10.0), which is close to the Re−O distance in tetrahedral ReO_4^- (1.73 Å). The presence of two types of Re−O bonds (Re−O_1 and Re−O_2), and one Re−Re bond, suggests both tetrahedral and octahedral-coordinated Re for pH 4.0 and pH 7.0. Between pH 1.0 and pH 10.0, the total N(Re−O) decreases from 6.0 ± 0.5 to 3.7 ± 0.3 (Table 1), while concomitantly N(Re−O_1) and N(Re−Re) decrease, and N(Re−O_2) increases. It is apparent that the local coordination environment of Re gradually changes from octahedral-coordinated Re(IV) to tetrahedral-coordinated Re(VII) as pH increases, in accord with less reduction.

SEM images, XPS spectra and XRD patterns were acquired to assess reduction of Re(VII) as a function of contact time with TCNS-P. As shown in Figure S7, the layered structure of Ti_2CT_x nanosheets in TCNS-P is retained after Re(VII) removal, though the porous 3D network partially collapses. Fitting of XPS spectra in the Re 4f region (Figure 5) indicates two sets of spin−orbit split doublets. The lines around 42.6 and 45.0 eV are assigned to Re(IV) $4f_{7/2}$ and Re(IV) $4f_{5/2}$, and the lines around 45.7 and 48.1 eV are assigned to Re(VII) $4f_{7/2}$ and Re(VII) $4f_{5/2}$, respectively.[69−71] The assignment of both Re(IV) and Re(VII) from XPS is consistent with the XANES and EXAFS results. As the contact time increased from 6 to 48 h, the Re(IV) fraction increased from approximately 30% to 85% (Figure 5), revealing that Re(VII) reduction is slower than adsorption, which achieves equilibrium within 1 h. High-resolution XPS spectra in the Ti 2p and O 1s regions (SI Figure S8) suggest that Ti_2CT_x in TCNS-P was gradually oxidized as Re(VII) was reduced, with evidence for loss Ti−C bonds and conversion of Ti−OH to Ti−O. Despite low crystallinity, the corrosion product of TCNS-P after 48 h reaction with Re(VII) can be roughly indexed to anatase (SI Figure S9), in agreement with our previous results.[40] As no Recontaining crystalline product was identified from the XRD patterns, we conclude that the reduced Re(IV) may be amorphous ReO_2.

Based on the combined results of sorption experiments and reaction product analysis, a postulated mechanism for removal of Re(VII) by TCNS-P is summarized as follows: Anionic ReO_4^- is first adsorbed on positively surface-charged TCNS-P via a fast electrostatic interaction. The Ti_2CT_x nanosheets then

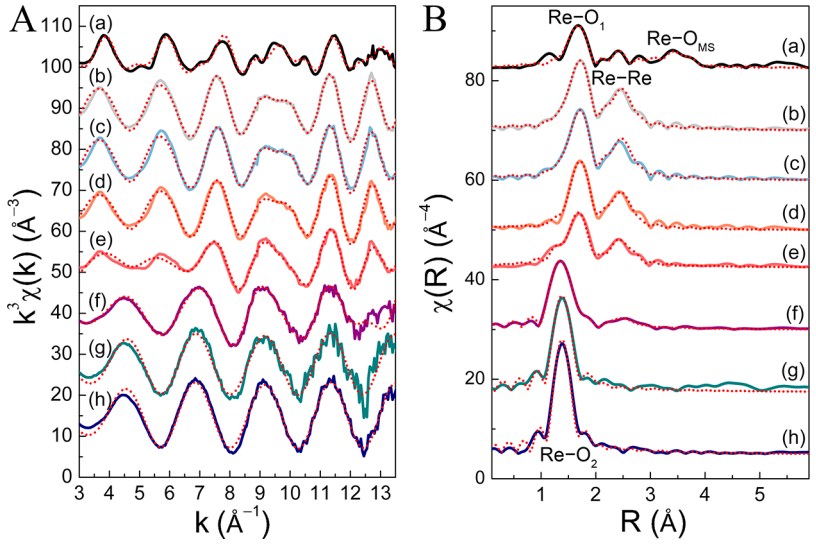

Figure 4. (A) Re L $_3$ edge k^3-weighted EXAFS spectra (solid lines) and the best theoretical fits (dotted lines) for rhenium-containing TCNS-P samples under different pH. (B) Corresponding nonphase shift corrected Fourier transforms. (a) ReO_2 reference; (b) pH 1.0; (c) pH 2.0; (d) pH 3.0; (e) pH 4.0; (f) pH 7.0; (g) pH 10.0; (h) Aqueous Re(VII) reference.

Table 1. Fitting Parameters from Least-Squares Fitting Analysis of EXAFS Spectra

sample	path	N[a]	R(Å)[b]	σ^2(Å^2)[c]	ΔE(eV)[d]	*R*-factor[e]
ReO_2	Re–O$_1$	6[f]	2.01 ± 0.01	0.002	11.2	0.031
	Re–Re	2[f]	2.57 ± 0.01	0.003		
	Re–O$_{MS}$	4[f]	3.89 ± 0.01	0.003		
pH 1.0	Re–O$_1$	6.0 ± 0.5	2.03 ± 0.01	0.003	8.7	0.007
	Re–Re	2.0 ± 0.5	2.58 ± 0.01	0.002		
pH 2.0	Re–O$_1$	6.0 ± 0.4	2.03 ± 0.01	0.003	9.3	0.012
	Re–Re	2.0 ± 0.5	2.58 ± 0.01	0.003		
pH 3.0	Re–O$_1$	4.7 ± 0.7	2.03 ± 0.01	0.001	9.1	0.017
	Re–Re	2.1 ± 0.9	2.58 ± 0.01	0.002		
pH 4.0	Re–O$_1$	4.0 ± 0.8	2.04 ± 0.01	0.001	10.9	0.014
	Re–O$_2$	1.5 ± 0.5	1.73 ± 0.01	0.002		
	Re–Re	1.4 ± 0.5	2.58 ± 0.01	0.002		
pH 7.0	Re–O$_1$	0.8 ± 0.3	2.09 ± 0.01	0.002	4.6	0.002
	Re–O$_2$	2.8 ± 0.2	1.71 ± 0.01	0.001		
	Re–Re	0.9 ± 0.6	2.58 ± 0.01	0.004		
pH 10.0	Re–O$_2$	3.7 ± 0.3	1.74 ± 0.01	0.001	10.1	0.011
Re(VII) (aq)	Re–O$_2$	4.0 ± 0.2	1.73 ± 0.01	0.001	9.9	0.014

[a]Coordination number. [b]Radial distance. [c]Debye–Waller factor. [d]Energy shift relative to the calculated Fermi level. [e]Goodness-of-fit indicator. [f]Fixed during fitting.

more gradually reduce some or most ReO_4^- to amorphous ReO_2 chains in the confined space, while Ti_2CT_x is partially oxidized to anatase.

Environmental Significance. Technetium contamination is a near-surface environmental remediation concern around legacy nuclear facilities due to the high mobility of Tc(VII). The demonstration here that surface-modified Ti_2CT_x nanosheets can significantly enhance adsorption of Re(VII), with ultimate reduction to insoluble ReO_2, suggests potential applications of TCNS-P for remediation of environmental Tc(VII). The standard redox potentials for Tc(VII) to Tc(IV) (+0.74 V) and Re(VII) to Re(IV) (+0.51 V) indicate that reduced Tc(IV) should be more stable compared to Re(IV).[7,72] Optimization here of conditions where Re(IV) dominates (e.g., pH 1–4) should guide development of applications of Ti_2CT_x-based materials for corresponding reduction of Tc(VII). TCNS-P has been demonstrated to behave as a slow-release electron donor, which could provide redox buffering for enhanced Tc immobilization compared with liquid reducing agents.[26] Identification of anatase as the product of Re(VII) reduction by Ti_2CT_x nanocomposite implies a stable matrix for sequestration of Tc(IV), which exhibits similar ionic radius

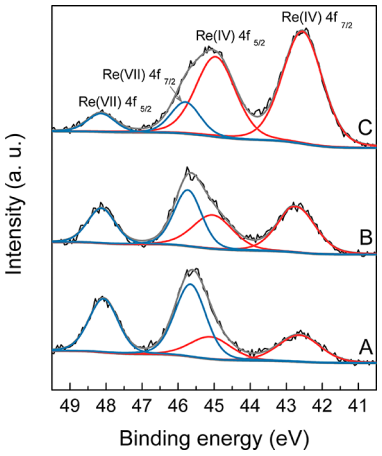

Figure 5. XPS spectra of rhenium-containing TCNS-P samples for different contact times at pH 3.0. (A) 6 h; (B) 24 h; (C) 48 h.

and octahedral coordination structures as Ti(IV).[65,73] The results for Re(VII) sequestration should motivate development of Ti-based MXenes as novel materials for reduction of Tc(VII) with in situ incorporation as Tc(IV).

AUTHOR INFORMATION

Corresponding Author

*Phone: +86-10-88233968; fax: +86-10-88238494; e-mail: shiwq@ihep.ac.cn.

ORCID

Lin Wang: 0000-0002-1539-9865

Liyong Yuan: 0000-0003-4261-8717

John K. Gibson: 0000-0003-2107-5418

Weiqun Shi: 0000-0001-9929-9732

Author Contributions

#L.W. and H.S. contributed equally to this work.

Notes

The authors declare no competing financial interest.

ACKNOWLEDGMENTS

This work was supported by the National Natural Science Foundation of China (Grants no. 21577144, 11675192, 21790373, and 21790370) and the Science Challenge Project (TZ2016004). Research of J.K.G. was supported by the Center for Actinide Science and Technology, an Energy Frontier Research Center funded by the U.S. Department of Energy, Office of Science, Basic Energy Sciences, under Award Number DE-SC0016568. We are grateful to the staff of Beijing Synchrotron Radiation Facility (BSRF) for EXAFS and XANES measurement.

REFERENCES

(1) Masters-Waage, N. K.; Morris, K.; Lloyd, J. R.; Shaw, S.; Mosselmans, J. F. W.; Boothman, C.; Bots, P.; Rizonlis, A.; Livens, F. R.; Law, G. T. W. Impacts of Repeated Redox Cycling on Technetium Mobility in the Environment. *Environ. Sci. Technol.* **2017**, *51*, 14301−14310.

(2) Fan, D. M.; Anitori, R. P.; Tebo, B. M.; Tratnyek, P. G.; Pacheco, J. S. L.; Kukkadapu, R. K.; Kovarik, L.; Engelhard, M. H.; Bowden, M. E. Oxidative Remobilization of Technetium Sequestered by Sulfide-Transformed Nano Zerovalent Iron. *Environ. Sci. Technol.* **2014**, *48*, 7409−7417.

(3) Peretyazhko, T.; Zachara, J. M.; Heald, S. M.; Kukkadapu, R. K.; Liu, C.; Plymale, A. E.; Resch, C. T. Reduction of Tc(VII) by Fe(II) sorbed on Al (hydr)oxides. *Environ. Sci. Technol.* **2008**, *42*, 5499−5506.

(4) Saslow, S. K.; Um, W.; Pearce, C. I.; Engelhard, M. H.; Bowden, M. E.; Lukens, W.; Leavy, I. I.; Riley, B. J.; Kirn, D. S.; Schweiger, M. J.; Kruger, A. A. Reduction and Simultaneous Removal of ^{99}Tc and Cr by $Fe(OH)_2(s)$ Mineral Transformation. *Environ. Sci. Technol.* **2017**, *51*, 8635−8642.

(5) Istok, J. D.; Senko, J. M.; Krumholz, L. R.; Watson, D.; Bogle, M. A.; Peacock, A.; Chang, Y. J.; White, D. C. In situ bioreduction of technetium and uranium in a nitrate-contaminated aquifer. *Environ. Sci. Technol.* **2004**, *38*, 468−475.

(6) Zhang, D. W.; Ronson, T. K.; Mosquera, J.; Martinez, A.; Nitschke, J. R. Selective Anion Extraction and Recovery Using a $Fe^{II}_4L_4$ Cage. *Angew. Chem., Int. Ed.* **2018**, *57*, 3717−3721.

(7) Maset, E. R.; Sidhu, S. H.; Fisher, A.; Heydon, A.; Worsfold, P. J.; Cartwright, A. J.; Keith-Roach, M. J. Effect of organic co-contaminants on technetium and rhenium speciation and solubility under reducing conditions. *Environ. Sci. Technol.* **2006**, *40*, 5472−5477.

(8) Goh, K. H.; Lim, T. T.; Dong, Z. Application of layered double hydroxides for removal of oxyanions: A review. *Water Res.* **2008**, *42*, 1343−1368.

(9) Zhu, L.; Zhang, L. J.; Li, J.; Zhang, D.; Chen, L. H.; Sheng, D. P.; Yang, S. T.; Xiao, C. L.; Wang, J. Q.; Chai, Z. F.; Albrecht-Schmitt, T. E.; Wang, S. Selenium Sequestration in a Cationic Layered Rare Earth Hydroxide: A Combined Batch Experiments and EXAFS Investigation. *Environ. Sci. Technol.* **2017**, *51*, 8606−8615.

(10) Gu, B. H.; Dowlen, K. E.; Liang, L. Y.; Clausen, J. L. Efficient separation and recovery of technetium-99 from contaminated groundwater. *Sep. Technol.* **1996**, *6*, 123−132.

(11) Gu, B. H.; Brown, G. M.; Bonnesen, P. V.; Liang, L. Y.; Moyer, B. A.; Ober, R.; Alexandratos, S. D. Development of novel bifunctional anion exchange resins with improved selectivity for pertechnetate sorption from contaminated groundwater. *Environ. Sci. Technol.* **2000**, *34*, 1075−1080.

(12) Ashley, K. R.; Whitener, G. D.; Schroeder, N. C.; Ball, J. R.; Radzinski, S. D. Sorption behavior of pertechnetate ion on Reillex (TM)-HPQ anion exchange resin from Hanford and Melton Valley tank waste simulants and sodium hydroxide sodium nitrate solutions. *Solvent Extr. Ion Exch.* **1998**, *16*, 843−859.

(13) Shen, J.; Chai, W.; Wang, K. X.; Zhang, F. Efficient Removal of Anionic Radioactive Pollutant from Water Using Ordered Urea-Functionalized Mesoporous Polymeric Nanoparticle. *ACS Appl. Mater. Interfaces* **2017**, *9*, 22440−22448.

(14) Li, J.; Dai, X.; Zhu, L.; Xu, C.; Zhang, D.; Silver, M. A.; Li, P.; Chen, L. H.; Li, Y. Z.; Zuo, D. W.; Zhang, H.; Xiao, C. L.; Chen, J.; Diwu, J.; Farha, O. K.; Albrecht-Schmitt, T. E.; Chai, Z. F.; Wang, S. A. $^{99}TcO_4^-$ remediation by a cationic polymeric network. *Nat. Commun.* **2018**, *9*, 3007.

(15) Zhu, L.; Xiao, C. L.; Dai, X.; Li, J.; Gui, D. X.; Sheng, D. P.; Chen, L. H.; Zhou, R. H.; Chai, Z. F.; Albrecht-Schmitt, T. E.; Wang, S. Exceptional Perrhenate/Pertechnetate Uptake and Subsequent Immobilization by a Low-Dimensional Cationic Coordination Polymer:

Overcoming the Hofmeister Bias Selectivity. *Environ. Sci. Technol. Lett.* **2017**, *4*, 316−322.
(16) Banerjee, D.; Elsaidi, S. K.; Aguila, B.; Li, B. Y.; Kim, D.; Schweiger, M. J.; Kruger, A. A.; Doonan, C. J.; Ma, S. Q.; Thallapally, P. K. Removal of Pertechnetate-Related Oxyanions from Solution Using Functionalized Hierarchical Porous Frameworks. *Chem. - Eur. J.* **2016**, *22*, 17581−17584.
(17) Sheng, D. P.; Zhu, L.; Xu, C.; Xiao, C. L.; Wang, Y. L.; Wang, Y. X.; Chen, L. H.; Diwu, J.; Chen, J.; Chai, Z. F.; Albrecht-Schmitt, T. E.; Wang, S. A. Efficient and Selective Uptake of TcO_4^- by a Cationic Metal-Organic Framework Material with Open Ag^+ Sites. *Environ. Sci. Technol.* **2017**, *51*, 3471−3479.
(18) Banerjee, D.; Xu, W. Q.; Nie, Z. M.; Johnson, L. E. V.; Coghlan, C.; Sushko, M. L.; Kim, D.; Schweiger, M. J.; Kruger, A. A.; Doonan, C. J.; Thallapally, P. K. Zirconium-Based Metal-Organic Framework for Removal of Perrhenate from Water. *Inorg. Chem.* **2016**, *55*, 8241−8243.
(19) Drout, R. J.; Otake, K.; Howarth, A. J.; Islamoglu, T.; Zhu, L.; Xiao, C. L.; Wang, S.; Farha, O. K. Efficient Capture of Perrhenate and Pertechnetate by a Mesoporous Zr Metal-Organic Framework and Examination of Anion Binding Motifs. *Chem. Mater.* **2018**, *30*, 1277−1284.
(20) Liu, W.; Wang, Y. L.; Bai, Z. L.; Li, Y. X.; Wang, Y. X.; Chen, L. H.; Xu, L.; Diwu, J.; Chai, Z. F.; Wang, S. Hydrolytically Stable Luminescent Cationic Metal Organic Framework for Highly Sensitive and Selective Sensing of Chromate Anions in Natural Water Systems. *ACS Appl. Mater. Interfaces* **2017**, *9*, 16448−16457.
(21) Zhu, L.; Sheng, D. P.; Xu, C.; Dai, X.; Silver, M. A.; Li, J.; Li, P.; Wang, Y. X.; Wang, Y. L.; Chen, L. H.; Xiao, C. L.; Chen, J.; Zhou, R. H.; Zhang, C.; Farha, O. K.; Chai, Z. F.; Albrecht-Schmitt, T. E.; Wang, S. Identifying the Recognition Site for Selective Trapping of $^{99}TcO_4^-$ in a Hydrolytically Stable and Radiation Resistant Cationic Metal-Organic Framework. *J. Am. Chem. Soc.* **2017**, *139*, 14873−14876.
(22) Arai, Y. J.; Powell, B. A.; Kaplan, D. I. Residence time effects on technetium reduction in slag-based cementitious materials. *J. Hazard. Mater.* **2018**, *342*, 510−518.
(23) Lukens, W. W.; Bucher, J. J.; Edelstein, N. M.; Shuh, D. K. Products of Pertechnetate Radiolysis in Highly Alkaline Solution: Structure of $TcO_2.xH_2O$. *Environ. Sci. Technol.* **2002**, *36*, 1124−1129.
(24) Shang, Y.; Xiao, J. X.; Weng, H. Q.; Li, F. H.; Cheng, S.; Yamashita, S.; Muroya, Y.; Lin, M. Z. Efficient separation of Re(VII) by radiation-induced reduction from aqueous solution. *Chem. Eng. J.* **2018**, *341*, 317−326.
(25) Fredrickson, J. K.; Zachara, J. M.; Plymale, A. E.; Heald, S. M.; McKinley, J. P.; Kennedy, D. W.; Liu, C. X.; Nachimuthu, P. Oxidative dissolution potential of biogenic and abiogenic TcO_2 in subsurface sediments. *Geochim. Cosmochim. Acta* **2009**, *73*, 2299−2313.
(26) Newsome, L.; Cleary, A.; Morris, K.; Lloyd, J. R. Long-Term Immobilization of Technetium via Bioremediation with Slow-Release Substrates. *Environ. Sci. Technol.* **2017**, *51*, 1595−1604.
(27) Burton-Pye, B. P.; Radivojevic, I.; McGregor, D.; Mbomekalle, I. M.; Lukens, W. W.; Francesconi, L. C. Photoreduction of Tc-99 Pertechnetate by Nanometer-Sized Metal Oxides: New Strategies for Formation and Sequestration of Low-Valent Technetium. *J. Am. Chem. Soc.* **2011**, *133*, 18802−18815.
(28) Chatterjee, S.; Hall, G. B.; Johnson, I. E.; Du, Y. G.; Walter, E. D.; Washton, N. M.; Levitskaia, T. G. Surprising formation of quasi-stable Tc(VI) in high ionic strength alkaline media. *Inorg. Chem. Front.* **2018**, *5*, 2081−2091.
(29) Zhang, X. X.; Zhao, Y. J.; Wei, Y. Z. Electrolytic reduction of Re(VII) using a flow type electrolysis cell and its possibility of radiopharmaceuticals application. *Nucl. Sci. Technol.* **2015**, *26*, 102−106.
(30) Newsome, L.; Morris, K.; Cleary, A.; Masters-Waage, N. K.; Boothman, C.; Joshi, N.; Atherton, N.; Lloyd, J. R. The impact of iron nanoparticles on technetium-contaminated groundwater and sediment microbial communities. *J. Hazard. Mater.* **2019**, *364*, 134−142.
(31) Darab, J. G.; Amonette, A. B.; Burke, D. S. D.; Orr, R. D.; Ponder, S. M.; Schrick, B.; Mallouk, T. E.; Lukens, W. W.; Caulder, D. L.; Shuh, D. K. Removal of pertechnetate from simulated nuclear waste streams using supported zerovalent iron. *Chem. Mater.* **2007**, *19*, 5703−5713.
(32) Liu, J.; Pearce, C. I.; Qafoku, O.; Arenholz, E.; Heald, S. M.; Rosso, K. M. Tc(VII) reduction kinetics by titanomagnetite $Fe_{3-x}Ti_xO_4$ nanoparticles. *Geochim. Cosmochim. Acta* **2012**, *92*, 67−81.
(33) Neeway, J. J.; Asmussen, R. M.; Lawter, A. R.; Bowden, M. E.; Lukens, W. W.; Sarma, D.; Riley, B. J.; Kanatzidis, M. G.; Qafoku, N. P. Removal of TcO_4^- from Representative Nuclear Waste Streams with Layered Potassium Metal Sulfide Materials. *Chem. Mater.* **2016**, *28*, 3976−3983.
(34) Pearce, C. I.; Icenhower, J. P.; Asmussen, R. M.; Tratnyek, P. G.; Rosso, K. M.; Lukens, W. W.; Qafoku, N. P. Technetium Stabilization in Low-Solubility Sulfide Phases: A Review. *ACS Earth Space Chem.* **2018**, *2*, 532−547.
(35) Levitskaia, T. G.; Chatterjee, S.; Pence, N. K.; Romero, J.; Varga, T.; Engelhard, M. H.; Du, Y. G.; Kovarik, L.; Arey, B. W.; Bowden, M. E.; Walter, E. D. Inorganic tin aluminophosphate nanocomposite for reductive separation of pertechnetate. *Environ. Sci.: Nano* **2016**, *3*, 1003−1013.
(36) Peng, J. H.; Chen, X. Z.; Ong, W. J.; Zhao, X. J.; Li, N. Surface and Heterointerface Engineering of 2D MXenes and Their Nanocomposites: Insights into Electro- and Photocatalysis. *Chem.* **2019**, *5*, 18−50.
(37) Anasori, B.; Lukatskaya, M. R.; Gogotsi, Y. 2D metal carbides and nitrides (MXenes) for energy storage. *Nat. Rev. Mater.* **2017**, *2*, 16098.
(38) Ng, V. M. H.; Huang, H.; Zhou, K.; Lee, P. S.; Que, W. X.; Xu, J. Z.; Kong, L. B. Recent progress in layered transition metal carbides and/or nitrides (MXenes) and their composites: synthesis and applications. *J. Mater. Chem. A* **2017**, *5*, 3039−3068.
(39) Zhang, Y. J.; Wang, L.; Zhang, N. N.; Zhou, Z. J. Adsorptive environmental applications of MXene nanomaterials: a review. *RSC Adv.* **2018**, *8*, 19895−19905.
(40) Wang, L.; Song, H.; Yuan, L. Y.; Li, Z. J.; Zhang, Y. J.; Gibson, J. K.; Zheng, L. R.; Chai, Z. F.; Shi, W. Q. Efficient U(VI) Reduction and Sequestration by Ti_2CT_x MXene. *Environ. Sci. Technol.* **2018**, *52*, 10748−10756.
(41) Wang, L.; Tao, W. Q.; Yuan, L. Y.; Liu, Z. R.; Huang, Q.; Chai, Z. F.; Gibson, J. K.; Shi, W. Q. Rational control of the interlayer space inside two-dimensional titanium carbides for highly efficient uranium removal and imprisonment. *Chem. Commun.* **2017**, *53*, 12084−12087.
(42) Mu, W. J.; Du, S. Z.; Yu, Q. H.; Li, X. L.; Wei, H. Y.; Yang, Y. C. Improving barium ion adsorption on two-dimensional titanium carbide by surface modification. *Dalton. Trans.* **2018**, *47*, 8375−8381.
(43) Wang, L.; Yuan, L. Y.; Chen, K.; Zhang, Y. J.; Deng, Q. H.; Du, S. Y.; Huang, Q.; Zheng, L. R.; Zhang, J.; Chai, Z. F.; Barsoum, M. W.; Wang, X. K.; Shi, W. Q. Loading Actinides in Multilayered Structures for Nuclear Waste Treatment: The First Case Study of Uranium Capture with Vanadium Carbide MXene. *ACS Appl. Mater. Interfaces* **2016**, *8*, 16396−16403.
(44) Mu, W.; Du, S.; Li, X.; Yu, Q.; Wei, H.; Yang, Y.; Peng, S. Removal of radioactive palladium based on novel 2D titanium carbides. *Chem. Eng. J.* **2019**, *358*, 283−290.
(45) Li, S. X.; Wang, L.; Peng, J.; Zhai, M. L.; Shi, W. Q. Efficient thorium(IV) removal by two-dimensional Ti_2CT_x MXene from aqueous solution. *Chem. Eng. J.* **2019**, *366*, 192−199.
(46) Voigt, C. A.; Ghidiu, M.; Natu, V.; Barsoum, M. W. Anion Adsorption, $Ti_3C_2T_z$ MXene Multilayers, and Their Effect on Claylike Swelling. *J. Phys. Chem. C* **2018**, *122*, 23172−23179.
(47) Ying, Y. L.; Liu, Y.; Wang, X. Y.; Mao, Y. Y.; Cao, W.; Hu, P.; Peng, X. S. Two-Dimensional Titanium Carbide for Efficiently Reductive Removal of Highly Toxic Chromium(VI) from Water. *ACS Appl. Mater. Interfaces* **2015**, *7*, 1795−1803.
(48) Yang, D. Q.; Rochette, J. F.; Sacher, E. Spectroscopic evidence for pi-pi interaction between poly(diallyl dimethylammonium) chloride and multiwalled carbon nanotubes. *J. Phys. Chem. B* **2005**, *109*, 4481−4484.
(49) Ling, Z.; Ren, C. E.; Zhao, M. Q.; Yang, J.; Giammarco, J. M.; Qiu, J. S.; Barsoum, M. W.; Gogotsi, Y. Flexible and conductive MXene

films and nanocomposites with high capacitance. *Proc. Natl. Acad. Sci. U. S. A.* **2014**, *111*, 16676−16681.
(50) Sheng, G. D.; Tang, Y. N.; Linghu, W. S.; Wang, L. J.; Li, J. X.; Li, H.; Wang, X. K.; Huang, Y. Y. Enhanced immobilization of ReO_4^- by nanoscale zerovalent iron supported on layered double hydroxide via an advanced XAFS approach: Implications for TcO_4^- sequestration. *Appl. Catal., B* **2016**, *192*, 268−276.
(51) Li, J.; Chen, C. L.; Zhang, R.; Wang, X. K. Reductive immobilization of Re(VII) by graphene modified nanoscale zero-valent iron particles using a plasma technique. *Sci. China: Chem.* **2016**, *59*, 150−158.
(52) Gao, Y.; Chen, K.; Tan, X. L.; Wang, X. L.; Alsaedi, A.; Hayat, T.; Chen, C. L. Interaction Mechanism of Re(VII) with Zirconium Dioxide Nanoparticles Archored onto Reduced Graphene Oxides. *ACS Sustainable Chem. Eng.* **2017**, *5*, 2163−2171.
(53) Alhabeb, M.; Maleski, K.; Anasori, B.; Lelyukh, P.; Clark, L.; Sin, S.; Gogotsi, Y. Guidelines for Synthesis and Processing of Two-Dimensional Titanium Carbide ($Ti_3C_2T_x$ MXene). *Chem. Mater.* **2017**, *29*, 7633−7644.
(54) Ravel, B.; Newville, M. ATHENA, ARTEMIS, HEPHAESTUS: data analysis for X-ray absorption spectroscopy using IFEFFIT. *J. Synchrotron Radiat.* **2005**, *12*, 537−541.
(55) Dong, L. L.; Zhang, X. Q.; Ren, S. X.; Lei, T. Z.; Sun, X. X.; Qi, Y. D.; Wu, Q. L. Poly(diallyldimethylammonium chloride)-cellulose nanocrystals supported Au nanoparticles for nonenzymatic glucose sensing. *RSC Adv.* **2016**, *6*, 6436−6442.
(56) Li, F. Y.; Yang, Q. Y.; Qiu, F.; Liu, Y. Modification of superparamagnetic iron oxide nanoparticles with poly-(diallyldimethylammonium chloride) at air atmosphere. *Polym. Adv. Technol.* **2016**, *27*, 1530−1534.
(57) Peng, Q. M.; Guo, J. X.; Zhang, Q. R.; Xiang, J. Y.; Liu, B. Z.; Zhou, A. G.; Liu, R. P.; Tian, Y. J. Unique Lead Adsorption Behavior of Activated Hydroxyl Group in Two-Dimensional Titanium Carbide. *J. Am. Chem. Soc.* **2014**, *136*, 4113−4116.
(58) Kamari, A.; Ngah, W. S. W.; Chong, M. Y.; Cheah, M. L. Sorption of acid dyes onto GLA and H_2SO_4 cross-linked chitosan beads. *Desalination* **2009**, *249*, 1180−1189.
(59) Zhao, Y. G.; Li, J. X.; Zhao, L. P.; Zhang, S. W.; Huang, Y. S.; Wu, X. L.; Wang, X. K. Synthesis of amidoxime-functionalized Fe_3O_4@SiO_2 core-shell magnetic microspheres for highly efficient sorption of U(VI). *Chem. Eng. J.* **2014**, *235*, 275−283.
(60) Mashtalir, O.; Cook, K. M.; Mochalin, V. N.; Crowe, M.; Barsoum, M. W.; Gogotsi, Y. Dye adsorption and decomposition on two-dimensional titanium carbide in aqueous media. *J. Mater. Chem. A* **2014**, *2*, 14334−14338.
(61) Custelcean, R.; Moyer, B. A. Anion separation with metal-organic frameworks. *Eur. J. Inorg. Chem.* **2007**, *2007*, 1321−1340.
(62) Gardner, J. S.; Peterson, Q. P.; Walker, J. O.; Jensen, B. D.; Adhikary, B.; Harrison, R. G.; Lamb, J. D. Anion transport through polymer inclusion membranes facilitated by transition metal containing carriers. *J. Membr. Sci.* **2006**, *277*, 165−176.
(63) Zhang, P. F.; Avudzega, D. M.; Bowman, R. S. Removal of perchlorate from contaminated waters using surfactant-modified zeolite. *J. Environ. Qual.* **2007**, *36*, 1069−1075.
(64) Roach, J. D.; Lane, R. F.; Hussain, Y. Comparative study of the uses of poly(4-vinylpyridine) and poly(diallyldimethylammonium) chloride for the removal of perchlorate from aqueous solution by polyelectrolyte-enhanced ultrafiltration. *Water Res.* **2011**, *45*, 1387−1393.
(65) Lukens, W. W.; Saslow, S. A. Aqueous Synthesis of Technetium-Doped Titanium Dioxide by Direct Oxidation of Titanium Powder, a Precursor for Ceramic Nuclear Waste Forms. *Chem. Mater.* **2017**, *29*, 10369−10376.
(66) Heald, S. M.; Krupka, K. M.; Brown, C. F. Incorporation of pertechnetate and perrhenate into corroded steel surfaces studied by X-ray absorption fine structure spectroscopy. *Radiochim. Acta* **2012**, *100*, 243−253.
(67) Tan, X. L.; Fang, M.; Ren, X. M.; Mei, H. Y.; Shao, D. D.; Wang, X. K. Effect of Silicate on the Formation and Stability of Ni-Al LDH at the gamma-Al_2O_3 Surface. *Environ. Sci. Technol.* **2014**, *48*, 13138−13145.
(68) Tan, X. L.; Ren, X. M.; Chen, C. L.; Wang, X. K. Analytical approaches to the speciation of lanthanides at solid-water interfaces. *TrAC, Trends Anal. Chem.* **2014**, *61*, 107−132.
(69) Okal, J.; Tylus, W.; Kepinski, L. XPS study of oxidation of rhenium metal on gamma-Al_2O_3 support. *J. Catal.* **2004**, *225*, 498−509.
(70) Jeong, Y. K.; Lee, Y. M.; Yun, J.; Mazur, T.; Kim, M.; Kim, Y. J.; Dygas, M.; Choi, S. H.; Kim, K. S.; Kwon, O. H.; Yoon, S. M.; Grzybowski, B. A. Tunable Photoluminescence across the Visible Spectrum and Photocatalytic Activity of Mixed-Valence Rhenium Oxide Nanoparticles. *J. Am. Chem. Soc.* **2017**, *139*, 15088−15093.
(71) Bare, S. R.; Kelly, S. D.; Vila, F. D.; Boldingh, E.; Karapetrova, E.; Kas, J.; Mickelson, G. E.; Modica, F. S.; Yang, N.; Rehr, J. J. Experimental (XAS, STEM, TPR, and XPS) and Theoretical (DFT) Characterization of Supported Rhenium Catalysts. *J. Phys. Chem. C* **2011**, *115*, 5740−5755.
(72) Sarri, S.; Misaelides, P.; Zamboulis, D.; Gaona, X.; Altmaier, M.; Geckeis, H. Rhenium(VII) and technetium(VII) separation from aqueous solutions using a polyethylenimine-epichlorohydrin resin. *J. Radioanal. Nucl. Chem.* **2016**, *307*, 681−689.
(73) Lukens, W. W.; Magnani, N.; Tyliszczak, T.; Pearce, C. I.; Shuh, D. K. Incorporation of Technetium into Spinel Ferrites. *Environ. Sci. Technol.* **2016**, *50*, 13160−13168.